NON-LINEAR EFFECTS OF INSERTION DEVICES: SIMULATION AND EXPERIMENT RESULTS *

A. Xiao, M. Borland, L. Emery, V. Sajaev
Argonne National Laboratory, Argonne, IL 60439, USA

Abstract

The Advanced Photon Source (APS) Upgrade includes adding more insertion devices (IDs) to the storage ring. Perturbations from IDs have been reviewed, with the most significant sources coming from IDs that generate circular polarized light. To address this, we measured non-linear effects from the existing circular polarized undulator (CPU) and intermediate-energy x-ray (IEX) undulator. Measurement results were compared with simulation results. Proposed correction schemes were tested experimentally.

INTRODUCTION

The ongoing APS Upgrade (APS-U) project includes installing IDs in unused straights and replacing some IDs with devices better-optimized for user requirements. ID perturbations to the beam can be qualitatively expressed by [1]

$$\Delta x'(x) \propto \frac{L_w}{E^2} K^2 \frac{d}{dx} F^2(x), \qquad (1)$$

where L_w is the length of the wiggler, E is the beam energy, K is the wiggler strength, and $F(x) = B_y(x)/B_y(0)$. Non-linear effects come from the roll-off in $F(x)$.

For planar IDs, only one on-axis field (typically B_y) needs to be non-zero. Thus a generally wider ID pole and flatter $F(x)$ is possible, which reduces non-linearities. For IDs that generate elliptical radiation, both B_x and B_y are necessarily non-zero on axis. The required magnet structure is much more complicated, with narrower poles and, as a consequence, larger variation of $F(x)$. Figure 1 illustrates this difference for some of the typical and planned APS IDs. ID parameters are listed in Table 1.

To better understand the beam dynamics effects of ID field non-linearity, several simulation methods have been implemented in `elegant` [2]. Some of the methods require an analytical wiggler field expansion, which can be obtained through fitting a 3D magnetic field map to a model. In this paper, we first describe these simulation tools, fitting methods, and methods to reduce artificial errors from fitting. Then, using IEX as an example, we show simulation results from a measured field map. Finally, we present some experimental results from CPU and IEX operations.

SIMULATION TOOLS AND FITTING METHOD

There are four elements in `elegant` that simulate IDs: CWIGGLER, GFWIGGLER, UKICKMAP, and FTABLE.

* Work supported by the U. S. Department of Energy, Office of Science, under Contract No. DE-AC02-06CH11357.

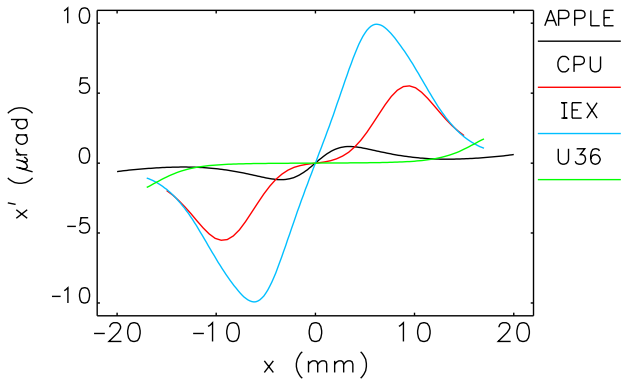

Figure 1: Comparison of simulated in-plane kick map ($y = 0$) for different types of IDs.

Table 1: Typical ID Parameters

ID Type	Length (m)	K_max+	By Pole Width (mm)
U33 *	2.4	2.75	51
U36 *	2.1	3.31	39.5
CPU*	1.8	2.77(H) 2.77(V) 2.5(C)	24
IEX*	4.75	5.27(H) 3.86(V) 3.86(C)	18.2
APPLE#	2.1	3.57(H) 2.7(V) 3.03(C)	35×35

+ H/V/C are different polarization mode for elliptical ID.
* Currently operated at APS.
# ID is under development, parameters are under consideration.

UKICKMAP uses kick maps [3] obtained from magnet design directly or from tracking results of the other three methods. All other methods use 3D field maps from ID design or field measurement. FTABLE uses the field map directly and is non-canonical, while CWIGGLER and GFWIGGLER require an analytical wiggler field expansion (from the 3D field map fitting) and are canonical. Our typical procedure for simulating nonlinear ID effects is: fit the 3D field map to a field expansion; using CWIGGLER or GFWIGGLER, track a bunch of particles through the element in a "grid" distribution on the $x - y$ plane with $x' = y' = 0$, and determine the kick map at the exit; use the kick map as input to UKICKMAP to perform various

ISBN 978-3-95450-138-0

simulations. The key to the entire procedure is fitting a field map to the field expansion. The general field expansion of an elliptical undulator is written as [4]:

$$\begin{aligned} B_x^H &= B_0^H \sum_{m,n} A_{mn}^H \frac{k_{x,mn}^H}{k_{y,mn}^H} \sin(k_{x,mn}^H x) \\ &\quad \cdot \sinh(k_{y,mn}^H y) \cdot \cos(k_{zn} z), \\ B_y^H &= -B_0^H \sum_{m,n} A_{mn}^H \cos(k_{x,mn}^H x) \\ &\quad \cdot \cosh(k_{y,mn}^H y) \cdot \cos(k_{zn} z), \end{aligned} \tag{2}$$

with $(k_{y,mn}^H)^2 = (k_{x,mn}^H)^2 + (k_{zn})^2$ for the field generated from the two middle poles, and

$$\begin{aligned} B_x^V &= B_0^V \sum_{m,n} A_{mn}^V \cos(k_{x,mn}^V x) \\ &\quad \cdot \cosh(k_{y,mn}^V y) \cdot \cos(k_{zn} z + \tfrac{\pi}{2}), \\ B_y^V &= B_0^V \sum_{m,n} A_{mn}^V \frac{k_{y,mn}^V}{k_{x,mn}^V} \sin(k_{x,mn}^V x) \\ &\quad \cdot \sinh(k_{y,mn}^V y) \cdot \cos(k_{zn} z + \tfrac{\pi}{2}), \end{aligned} \tag{3}$$

with $(k_{y,mn}^V)^2 = (k_{x,mn}^V)^2 + (k_{zn})^2$ for the field generated from the four side poles. Here, $k_{zn} = 2\pi n/\lambda_u$, λ_u is the period, and B_0^H and B_0^V are the maximum on-axis horizontal and vertical fields, respectively. The total field is given by

$$\begin{aligned} B_y^C &= B_y^H + B_y^V \\ B_x^C &= B_x^H + B_x^V . \end{aligned} \tag{4}$$

ID field profiles greatly differ from a pure sinusoidal shape and have high harmonic components, making direct fitting very difficult. We thus developed a linear fit method. First, the field data are fit to longitudinal harmonics:

$$\begin{aligned} B_x^C &= \sum_n G_{H,n} \cdot \cos(k_{zn} z) + \sum_n G_{V,n} \cdot \cos(k_{zn} z), \\ B_y^C &= \sum_n F_{H,n} \cdot \cos(k_{zn} z) + \sum_n F_{V,n} \cdot \cos(k_{zn} z), \end{aligned} \tag{5}$$

where $\cos(k_{zn} z)$ are known values at each data point, and $F_{H/V,n}$ and $G_{H/V,n}$ are fit parameters. These F and G parameters are in turn decomposed into transverse harmonics following

$$\begin{aligned} F_{H,n} &= \sum_m \left[-B_0^H A_{mn}^H \cdot \cosh(k_{y,mn}^H y) \right] \cdot \cos(k_{x,mn}^H x) \\ &= \sum_m f_{H,n,m} \cdot \cos(k_{x,mn}^H x). \end{aligned} \tag{6}$$

Note that $k_{y,mn}^H$ and $k_{x,mn}^H$ are still related. Both $k_{x,mn}^H$ and A_{mn}^H are unknown parameters to be fitted. In order to turn this into a linear fit, we give an initial value to $k_{x,mn}^H$, then fit $f_{H,n,m}$. The proper $k_{x,mn}^H$ value is obtained by scanning $k_{x,mn}^H$ over a suitable range and choosing the value that gives the smallest residuals. The same technique is applied to the other F and G parameters.

Depending on the original field data errors and the available field map region, the fit results may be invalid. The F and G coefficients are interrelated via Maxwell's equations, so fitting one will give the other. Usually we fit F_H and G_V as they give the non-zero on-axis field. In the case of large (measured or modeled) field errors, this results in large field errors at the boundary of the available field map. Fitting F and G parameters together will eliminate such errors (see Figure 2). For best results, the field map region

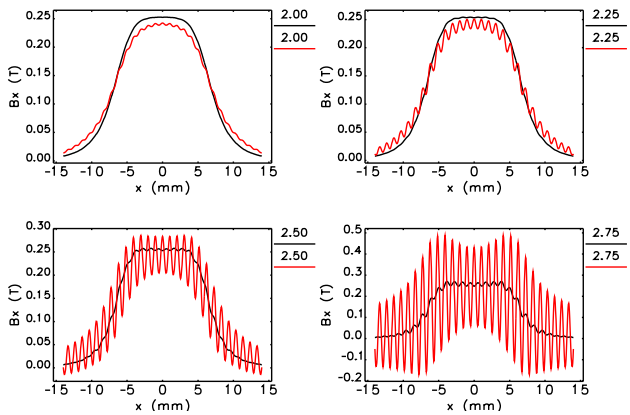

Figure 2: Fitted field profile at different y positions (legend value in mm). Red — fit F_H and G_V only; black — fit all F and G. Large fitting errors appears near the field map boundary.

should extend well beyond the expected dynamic aperture (DA). If an adequate field map region is unavailable, which we encountered in our EMVPU [5] simulation, we must use fewer small transverse harmonics (m) or manually set up boundary conditions that will help constrain the fitting results (see Figure 3).

SIMULATION RESULTS AND BEAM TEST

Figure 1 shows that IEX presents the strongest nonlinearity among all IDs that have been installed in the APS. Thus, detailed simulations were made with both designed and measured field maps. Due to large errors represented in the measured field data, the measured field map was fitted to its design model by adjusting its alignment (x, y, z), peak field (B_0), and roll-off parameter K_x slightly away from the value of the model simulation. Fitting results show that $K_{x,meas} \approx 0.96 K_{x,design}$. A slightly larger magnet field roll-off appears in the real device (see Figure 4). To include field errors, the IEX was sliced into several segments, each segment containing several periods. The error field was represented by a kick map at the end of each segment, calculated using the first field integral of the same

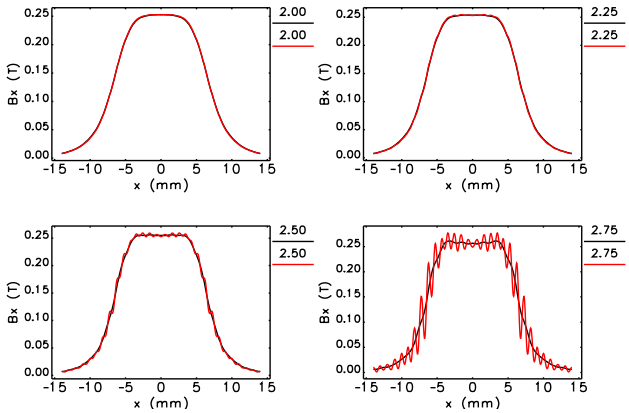

Figure 3: Fitted field profile at several y positions (legend value in mm). Black — harmonic m up to 30; red — harmonic m up to 50.

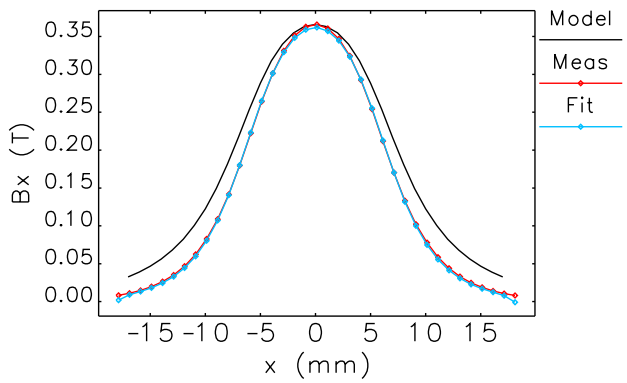

Figure 4: Peak Bx filed profile vs. x. Black — designed model; red — measured data; blue — fitted model.

segment. Simulated DA results for various conditions are shown in Figure 5. The simulation results predicted that the APS DA would be reduced slightly by IEX operation. This was confirmed by our beam-based measurements, as seen in Figure 6.

Another device with strong non-linearity is the Circularly Polarizing Undulator (CPU), for which we have a model field map, but no measured one. The non-linearity of the ideal CPU model is weaker than IEX, but the measured beam perturbations, such as orbit, tune, and coupling variations, indicate some larger field errors. The measured DA reduction from the CPU is also more severe than the IEX (see Figure 6). Unfortunately, we cannot simulate these field errors as we have no measured field map.

SUMMARY

Simulation of ID nonlinear effects can be accomplished in several ways. This paper explains how a field map can be fit to a field expansion used by `elegant` and what precautions are required for a valid result. Using the IEX device as an example, we illustrated how a measured field map was used to check the field quality and for DA simulation. Experimental results from both CPU and IEX operation show the importance of such simulation work.

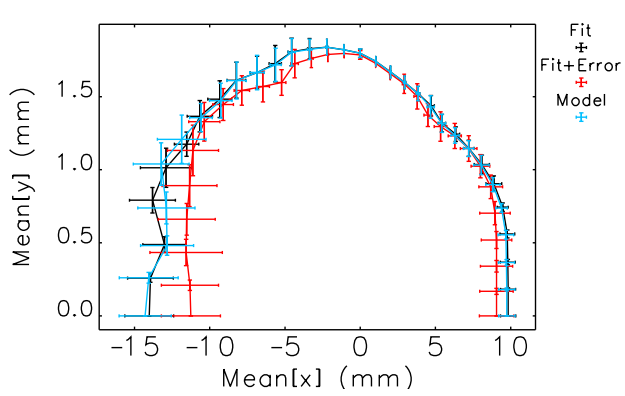

Figure 5: Dynamic aperture with machine errors. Black — field map from magnet measurement (fitted model); red — fitted model + measured field errors; blue — field map from IEX design.

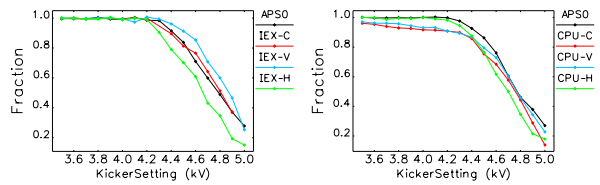

(a) IEX—DA is decreased at large kick strength

(b) CPU—DA is decreased from small kick strength

Figure 6: A fraction of beam survived after a kicker pulse vs kicker strength (DA) for the APS baseline (APS0 — CPU and IEX are off), and CPU or IEX running at different polarization modes (H/V/C).

REFERENCES

[1] J. Safranek et al., "Nonlinear dynamics in a SPEAR wiggler," Phys. Rev. ST Accel. Beams, 5, (2002), 010701.

[2] M. Borland, ANL/APS/LS-287 (2000).

[3] P. Elleaume, "A New Approach to the Electron Beam Dynamics in Undulators and Wigglers," Proc. of EPAC'92, p. 661 (1992); http://www.JACoW.org

[4] A. Xiao et al., Proc. PAC11, WEP064, p. 1594 (2011); http://www.JACoW.org

[5] M. Jaski, private communication.

ISBN 978-3-95450-138-0